PHYSICAL REVIEW B **86**, 235435 (2012)

Nonlinear damping in graphene resonators

Alexander Croy,* Daniel Midtvedt, Andreas Isacsson, and Jari M. Kinaret
Department of Applied Physics, Chalmers University of Technology, S-412 96 Göteborg, Sweden
(Received 5 April 2012; revised manuscript received 12 October 2012; published 20 December 2012)

Based on a continuum mechanical model for single-layer graphene, we propose and analyze a microscopic mechanism for dissipation in nanoelectromechanical graphene resonators. We find that coupling between flexural modes and in-plane phonons leads to linear and nonlinear damping of out-of-plane vibrations. By tuning external parameters such as bias and ac voltages, one can cross over from a linear- to a nonlinear-damping dominated regime. We discuss the behavior of the effective quality factor in this context.

DOI: 10.1103/PhysRevB.86.235435 PACS number(s): 72.80.Vp, 62.25.−g, 81.05.U−, 85.85.+j

I. INTRODUCTION

Advances in fabrication and detection techniques have enabled a wide range of experimental realizations of carbon-based nanoelectromechanical (NEM) resonators.[1–4] However, to optimize their operation, an increased understanding of dissipation mechanisms is needed. For NEM resonators in general, several processes leading to linear damping (LD) have been investigated.[5–8] Specifically, for graphene, at high temperatures, Ohmic losses in the metallic gate and the graphene sheet have been argued to limit the quality factor.[9] Recently, the focus has shifted to study quantum aspects of mechanical motion,[10,11] such as mechanical cat states,[12] which require a more detailed understanding of dissipation and decoherence mechanisms.

Since graphene-based resonators exhibit nonlinear behavior, one can expect the damping also to be amplitude dependent.[13–15] Nonlinear damping (NLD) was reported in recent experiments on graphene and carbon nanotube resonators.[4] However, little is known about the underlying physical mechanism, and typically phenomenological models are employed.[13–15] In these models, the resonator is coupled to a bath of harmonic oscillators. For couplings that depend quadratically on the resonator amplitude, it is known that NLD emerges.[13,16,17]

For carbon-based resonators, such a coupling naturally arises if the strain couples linearly to the degrees of freedom of some subsystem, which can be regarded as a bath. Two examples are the interaction between phonons and electrons[18,19] and the coupling of mechanical modes. The relative importance of the two mechanisms is *a priori* not known and will also depend on the details of the experimental realization.

In order to quantify the importance of the mechanical dissipation channel for NLD, we analyze the coupling between flexural modes and in-plane phonons. We show that it leads to a quadratic coupling and, consequently, to both LD and NLD. Whether LD or NLD dominates is determined by the ratio of vibrational amplitude and static deflection. We give an estimate for the expected crossover between LD and NLD, which can be experimentally verified.

II. MODEL AND METHOD

We consider a graphene sheet of length L and breadth b, suspended over a trench of width ℓ (cf. Fig. 1). The van der Waals attraction between the graphene and the substrate clamps down the sheet outside the suspended region.[20–22]

The trench is modeled by allowing the sheet to freely displace vertically in this region. Since out-of-plane displacement is accompanied by in-plane stretching or compression, flexural motion is converted into in-plane phonons in the suspended region. The clamping constrains the out-of-plane motion over the substrate, but still allows for small in-plane displacements. Consequently, in-plane phonons created in the suspended region transport energy away from this region. In contrast to a phenomenological modeling approach, we can relate dissipation to specific properties of the substrate and the graphene-substrate coupling. These properties can be obtained independently by theoretical or experimental means.

The dynamics of graphene NEM resonators are well described by the continuum theory of two-dimensional (2D) membranes.[23] For a resonator made from a sheet lying in the xy plane, this theory is conveniently formulated in terms of the in-plane displacement fields $u(x,y), v(x,y)$ in the x and y directions, respectively, and the displacement field in the z direction, $w(x,y)$. The equations of motion follow from the free energy $\mathcal{F} = \int dx\, dy\, [\mathcal{F}_b + \mathcal{F}_s]$ where $\mathcal{F}_b = \frac{\kappa}{2}|\Delta w|^2$ is the free energy density associated with pure bending and $\mathcal{F}_s = \frac{1}{2}\sum_{i,j}\sigma_{ij}\epsilon_{ij}$ is associated with stretching of the membrane. The symmetric 2D strain and stress tensors are here defined as

$$\epsilon_{xx} = u_{,x} + w_{,x}^2/2, \quad 2\epsilon_{xy} = (u_{,y} + v_{,x}) + w_{,x}w_{,y}, \quad \epsilon_{yy} = v_{,y} + w_{,y}^2/2, \tag{1a}$$

and

$$\sigma_{xx} = (\lambda_G + 2\mu_G)\epsilon_{xx} + \lambda_G\epsilon_{yy}, \quad \sigma_{xy} = 2\mu_G\epsilon_{xy}, \quad \sigma_{yy} = (\lambda_G + 2\mu_G)\epsilon_{yy} + \lambda_G\epsilon_{xx}\ , \tag{1b}$$

respectively. Spatial derivatives are denoted by subscripts, i.e., $u_{,x} = \partial u/\partial x$. The expression for the free energy, which is similar to that for large deflections of a plate,[24] contains three material parameters, the bending energy $\kappa \approx 1.1$–1.6 eV, and the Lamé parameters $\mu_G \approx 146$ N/m and $\lambda_G \approx 48$ N/m for graphene.[25–28] To study qualitatively the effect of phonon radiation into the supporting substrate, we assume for simplicity a quasi-one-dimensional (1D) situation where variations in the y direction are disregarded. This would be valid for a wide sheet where deviations from this assumption are confined to the regions around the edges. In this case, we have only the displacement fields $u(x,t)$ and $w(x,t)$. In any realistic functioning device, there is some small amount of built-in strain. In practice, this implies that the energy contribution from the bending energy is always negligible for the

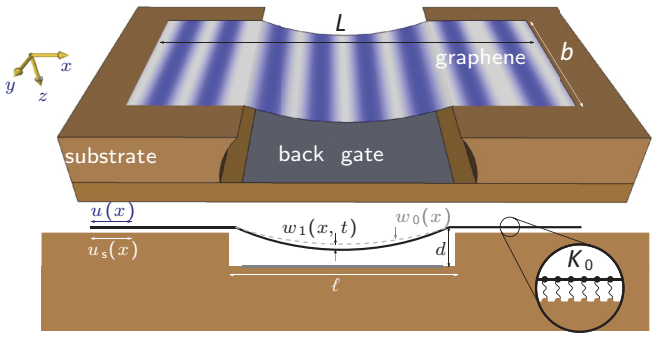

FIG. 1. (Color online) Schematic view of a suspended graphene membrane over a trench in an insulating substrate. A metallic gate is used for actuating the resonator. In-plane phonons are created in the suspended region and dissipate energy as they propagate away.

lowest-lying flexural modes.[27] Hence, to a good approximation we have for the quasi-1D graphene resonator attached to a substrate the free energy density

$$\mathcal{F}(x,y) = \frac{T_1}{2}\left(u_{,x}^2 + u_{,x}w_{,x}^2 + \frac{1}{4}w_{,x}^4\right) + \frac{1}{2}K(x)(u-u_S)^2 + \mathcal{E}_{\rm ext}[w], \quad (2)$$

where we have defined $T_1 = \lambda_G + 2\mu_G$. The potential $\mathcal{E}_{\rm ext}[w]$ accounts for interactions used to actuate the resonator. The second to last term couples the graphene displacement to the substrate displacement $u_S(x,y)$ in a harmonic approximation,[29] which largely allows us to obtain an analytical description.

The function $K(x)$ restricts this coupling to the supported region, i.e., $K(x) = K_0\Theta(|x| - \ell/2)$ with Θ being the Heaviside step function. The substrate is modeled as an elastic half-space and displacement at the surface $\vec{s}(\vec{x},z=0,t) = (u_S, v_S, w_S)$ is given in terms of a response function[24,30,31]

$$s_\mu(\vec{x},z=0,\omega) = -\sum_\nu \int \frac{d^2x'}{(2\pi)^2} R_{\mu\nu}(\vec{x}-\vec{x}',\omega)\sigma_{\nu z}(\vec{x}',\omega). \quad (3)$$

Consistent with the 1D model of the graphene sheet, only $\overline{u}_S(x) \equiv \int_{-b/2}^{b/2} dy\, u_S(x,y)$ is considered. Within the harmonic approximation, $\sigma_{xz} = K(x)(u-u_S)$.

The free energy (2) leads to a coupling between flexural vibrations and in-plane motion via the coupling energy $\mathcal{E}_{\rm coup} = (T_1/2)u_{,x}w_{,x}^2$, which is nonlinear in the flexural vibration amplitude. This coupling leads to NLD of the flexural vibrations.[13,15–17]

A. Equations of motion

The equations of motion for the out-of-plane and in-plane vibrations resulting from Eq. (2) are

$$\rho_G\ddot{w} - \frac{T_1}{2}\frac{d}{dx}\left(2u_{,x}w_{,x} + w_{,x}^3\right) = f_{\rm dc} + f_{\rm ac}\cos(\Omega t)\,, \quad (4a)$$

$$\rho_G\ddot{u} - \frac{T_1}{2}\frac{d}{dx}\left(2u_{,x} + w_{,x}^2\right) = -K(x)(u-\overline{u}_S/b), \quad (4b)$$

where $f_{\rm dc}(x)$ and $f_{\rm ac}(x)\cos(\Omega t)$ are the static and time-dependent parts of the actuation force. Typically, electrostatic actuation is used, resulting from a time-dependent back-gate voltage of the form $V_{\rm bg}(t) = V_{\rm dc} + V_{\rm ac}\cos(\Omega t)$ with $V_{\rm dc} \gg V_{\rm ac}$. To simplify the analysis, we assume the equilibrium stress field resulting from $f_{\rm dc}$ to be spatially uniform and equal to the tensile stress T_0 on the boundary.[24] Generally, at a given back-gate bias voltage, the resonance frequency $\Omega_0(V_{\rm dc})$ depends on initial stress and contains a shift due to electrostatic forces. This so-called tuning behavior will be further discussed in Sec. III A.

Since Eq. (4b) is linear in u, the influence of the environment can be accounted for by a Green's function embedding technique. The solution

$$u(x,t) = \int dx' \int dt' G(x,x',t-t')\frac{c^2}{2}\frac{d}{dx'}w_{,x'}{}^2(x',t') \quad (5)$$

is given in terms of the in-plane response function G, which contains information about the attachment to the substrate via Eq. (3). The speed of sound in graphene is denoted by $c = \sqrt{T_1/\rho_G}$, where ρ_G is the mass density of graphene.

B. Flexural mode dynamics

Next, we consider the fundamental flexural mode and set $w(x,t) = q(t)\phi(x)$ for $|x| \leqslant \ell/2$ and zero otherwise. The mode shape ϕ is normalized to the length of the resonator. Upon projecting Eq. (4a) onto the fundamental mode, an ordinary differential equation for the vibration amplitude q is obtained. Further, moving to a rotating frame, we write $q(t) = \{q_0 + \frac{1}{2}[q_1(t)e^{i\Omega t} + q_1^*(t)e^{-i\Omega t}]\}$ and $\dot{q}(t) = \frac{i\Omega}{2}[q_1(t)e^{i\Omega t} - q_1^*(t)e^{-i\Omega t}]$. Inserting these expressions into the equation of motion and performing the averaging yields an equation for the slowly varying amplitude q_1 [13], which contains memory terms related to linear and nonlinear damping. As the time scales for flexural motion and in-plane phonons are well separated ($\Omega_0 \ll c/\ell$), the memory terms can be eliminated. This procedure corresponds to a Markov approximation.[13] It is convenient to define new quantities

$$\hat{\chi}(\Omega) = \frac{c^2}{2}\int_{-l/2}^{l/2} dx \int_{-l/2}^{l/2} dx' \frac{d}{dx}\left[\phi_{,x}^2\hat{G}(x,x',-\Omega)\right]\frac{d}{dx'}\phi_{,x'}^2, \quad (6)$$

where $\hat{G}(x,x',\omega) = (2\pi)^{-1}\int d\tau\, G(x,x',\tau)e^{i\omega\tau}$ is the Fourier transform of the in-plane response function.

We obtain an equation of motion for the complex envelope function

$$m\dot{q}_1 = \left[im(\Omega_0-\Omega)q_1 + i\frac{3}{8}\frac{\alpha}{\Omega_0}|q_1|^2q_1 - \frac{1}{2}\gamma q_1 - \frac{1}{8}\eta|q_1|^2q_1 - \frac{i}{2\Omega_0}g\right]. \quad (7)$$

For finite temperatures, this equation has to be supplemented by noise forces, satisfying the fluctuation-dissipation relations. The thermally induced vibrations can lead to an additional broadening of the response curves.[13,32] In order to obtain a lower bound of LD and NLD, we will work in the limit of zero temperature. In Eq. (7), the coefficients $m = \rho_G\ell b$, α, γ, and η denote the suspended mass, the Duffing elastic constant,

linear and nonlinear damping, respectively. They are given in terms of $\hat{\chi}$ as follows:

$$\alpha = \alpha_0 - \frac{T_1 b}{2}\frac{4}{3}\mathrm{Re}\left(\hat{\chi}(0) + \frac{1}{2}\hat{\chi}(2\Omega)\right), \tag{8a}$$

$$\gamma = -\frac{T_1 b}{2\Omega_0} q_0^2\, 4\,\mathrm{Im}\,\hat{\chi}(\Omega), \tag{8b}$$

$$\eta = -\frac{T_1 b}{2\Omega_0}\, 2\,\mathrm{Im}\,\hat{\chi}(2\Omega). \tag{8c}$$

Here, the bare Duffing constant is given by $\alpha_0 = (T_1 b/2)\int dx\, \phi_{,x}(x)^4$. The driving strength is $g = \int dx\, \phi(x) f_{\mathrm{ac}}(x)$. In accordance with our previous simplifications, we neglect the small polaronic shift of Ω_0, which is proportional to Re $\hat{\chi}$, and an additional shift of α due to the broken symmetry in the presence of static deflection. Equation (7) is similar to the equations used to model NLD in micromechanical resonators[14,15] and recent experiments on carbon-based resonators,[4] the difference being the dependence of the damping coefficients in Eq. (8) on the driving frequency.

In Eq. (7), the prevailing damping mechanism is determined by the ratio

$$\tilde{\delta} \equiv \frac{\eta |q_1|^2}{4\gamma} \approx \frac{\mathrm{Im}\,\hat{\chi}(2\Omega)}{8\,\mathrm{Im}\,\hat{\chi}(\Omega)} \frac{\left|q_1^{\max}\right|^2}{q_0^2}. \tag{9}$$

Here, $|q_1^{\max}|$ denotes the maximum amplitude of the response for a given driving strength. Thus, $\tilde{\delta}$ is determined by the ratio of the overlap integrals defined in Eq. (6), which are purely geometrical quantities, and the ratio between the vibrational amplitude and the static deflection. For a small static deflection, it is therefore expected that NLD dominates the damping caused by phonon radiation. Similarly, the dimensionless ratio

$$\tilde{\eta} = \frac{\eta\ \Omega_0}{\alpha} \tag{10}$$

measures the relative importance of the two nonlinearities in Eq. (7).[14] For $\tilde{\eta} < \sqrt{3}$, the well-known bifurcation of the Duffing equation is present, while for $\tilde{\eta} > \sqrt{3}$ this bifurcation vanishes. The ratio $\tilde{\eta}$ is also a purely geometrical factor, apart from the weak dependence of Ω_0 on the static deformation of the graphene.

C. Numerical method

To compute the overlap integrals (6), we first consider the Fourier-transformed response of the substrate (3):

$$\begin{aligned}\overline{u}_{\mathrm{S}}(x,\omega) &= -\int_{-L/2}^{L/2}\frac{dx'}{(2\pi)^2}\int_{-b/2}^{b/2}dy'\int_{-b/2}^{b/2}dy \\ &\quad\times R_{xx}(x-x',y-y',\omega)\sigma_{xz}(x',y',\omega) \\ &\approx -\int_{-L/2}^{L/2}\frac{dx'}{(2\pi)^2}\overline{R}_{xx}(x-x',\omega)\,\overline{\sigma}_{xz}(x',\omega).\end{aligned} \tag{11}$$

In the second step, in order to get a purely 1D response function, we have approximated the y' dependence of $\sigma_{xz}(x',y')$ by the mean value $\frac{1}{b}\overline{\sigma}_{xz}$ and defined $\overline{R}_{xx}(x-x',\omega) \equiv \frac{1}{b}\int_{-b/2}^{b/2}dy'\int_{-b/2}^{b/2}dy\, R_{xx}(x-x',y-y',\omega)$.[33] The response function $R_{\mu\nu}$ for an elastic half-space is known analytically[24,30,31] and mainly depends on the longitudinal and transversal sound velocities of the substrate (see Appendix A).

Evaluating Eq. (11) at discrete positions $\{x_i\}_1^N$ leads to the linear system

$$\mathbb{K}\,\mathbf{u}_{\mathrm{S}}(\omega) = -[\mathbb{I} - \mathbb{K}\,\mathbb{R}(\omega)]^{-1}\mathbb{K}\,\mathbb{R}(\omega)\mathbb{K}\,\mathbf{u}(\omega), \tag{12}$$

which can be solved for $\overline{u}_{\mathrm{S}}(x_i,\omega)$. Here, boldface symbols denote vectors of length N, e.g., $\mathbf{u} = [u(x_1),\ldots,u(x_N)]$ and open face symbols are $N\times N$ matrices. In particular, $\mathbb{I}_{ij} = \delta_{i,j}$, $\mathbb{K}_{ij} = K(x_i)\delta_{i,j}$, and $\mathbb{R}_{ij} = (2\pi)^{-2}\overline{R}_{xx}(x_i - x_j,\omega)$. Using this result and the discretized version of the equation of motion (4b), one obtains an equation for the in-plane response function $\mathbb{G}_{ij} = \hat{G}(x_i,x_j,\omega)$:

$$\left[-\omega^2\mathbb{I} - c^2\mathbb{L} + \frac{1}{\rho_{\mathrm{G}}}[\mathbb{I} - \mathbb{K}\mathbb{R}(\omega)]^{-1}\mathbb{K}\right]\mathbb{G}(\omega) = \mathbb{I}, \tag{13}$$

where $\mathbb{L}$ is the discrete second derivative.[34] Approximating the integrations in Eq. (6) by numerical quadratures, one finally obtains

$$\hat{\chi}(\Omega) = \frac{c^2}{2}\mathbf{\Phi}^{\mathrm{t}}\mathbb{G}(-\Omega)\mathbf{\Phi} \tag{14}$$

with $\mathbf{\Phi}_i = \frac{d}{dx}\phi_{,x}^2|_{x=x_i}$, which allows the computation of $\hat{\chi}$ for a given geometry. The parameters entering the equation of motion can then be calculated using Eqs. (8). Following Ref. 14, we set $\tilde{\gamma} = \gamma/(m\Omega_0)$, $\tilde{\eta} = \eta\Omega_0/\alpha$, $\tilde{g} = g\sqrt{\frac{\alpha}{m^3}}/\Omega_0^3$, $\tilde{\Omega} = \Omega/\Omega_0$, and $\tilde{q} = q\sqrt{\alpha/m\Omega_0^2}$. In the limit of weak LD, $\tilde{\gamma} \ll 1$, the response of the resonator is determined solely by the dimensionless parameters $\tilde{\eta}$, $\tilde{g}$, and $\tilde{\Omega}$, describing the nonlinear damping, the driving strength, and the driving frequency.

III. RESULTS

To quantify the influence of LD and NLD, we consider the setup shown in Fig. 1 with a back-gate voltage $V_{\mathrm{bg}} = V_{\mathrm{dc}} + V_{\mathrm{ac}}\cos(\Omega t)$. The fundamental-mode shape is taken to be $\phi(x) = \sqrt{2}\cos(\pi x/\ell)$, which gives $\alpha_0 = 3T_1\pi^4 b/(4\ell^3)$. Within a parallel plate model for electrostatic actuation, the force acting on the graphene sheet is given by

$$\begin{aligned}f(x) &= \frac{\partial}{\partial w}\frac{1}{2}C(w)V_{\mathrm{bg}}^2 \\ &\approx -\frac{\epsilon_0}{2[d+q(t)\phi(x)]^2}\left[V_{\mathrm{dc}}^2 + 2V_{\mathrm{dc}}V_{\mathrm{ac}}\cos(\Omega t)\right],\end{aligned} \tag{15}$$

where $C(w) = \epsilon_0/(d+w)$ is the capacitance of a parallel plate capacitor with plates being separated by the distance $d+w$ and ϵ_0 is the vacuum permittivity. The distance is determined by the depth d of the trench and the flexural displacement w of the resonator. In the second line, we further assumed $V_{\mathrm{dc}} \gg V_{\mathrm{ac}}$, which is typically found in experiments. The force can be separated into a static and a time-dependent part $f = f_{\mathrm{dc}} + f_{\mathrm{ac}}\cos(\Omega t)$ with $f_{\mathrm{dc}} \propto V_{\mathrm{dc}}^2$ and $f_{\mathrm{ac}} \propto V_{\mathrm{dc}}V_{\mathrm{ac}}$, respectively. Since the displacement, which is on the order of a few nanometers, is much smaller than the trench depth, the force can be expanded in powers of w. Accordingly, the driving strength in Eq. (7) becomes $g = 2\sqrt{2}\ell b\epsilon_0 V_{\mathrm{dc}}V_{\mathrm{ac}}/(\pi d^2)$. Moreover, the static displacement can be found by solving Eqs. (4a) and (4b) in the static limit (see Appendix B). This yields $q_0 \approx \sqrt{2}\ell^2\epsilon_0 V_{\mathrm{dc}}^2/(\pi^3 d^2 T_0)$. Note the dependence on the

TABLE I. Graphene and resonator parameters used for the calculations in Figs. 3 and 4. Graphene and substrate parameters are taken from Refs. 35 and 36.

Graphene and substrate parameters		
Graphene mass density	ρ_G	7.6×10^{-7} kg m^{-2}
$\lambda_G + 2\mu_G$	T_1	340 N m^{-1}
SiO_2 mass density	ρ_S	2.2×10^3 kg m^{-3}
SiO_2 sound velocities	c_L/c	0.28
	c_T/c	0.18
Coupling strength	K_0	1.82×10^{20} N m^{-3}
Resonator parameters		
Total length	L	2 μm
Length	ℓ	1 μm
Width	b	1 μm
Distance to gate	d	330 nm
Tensile stress	T_0	0.34 N m^{-1}

tensile stress T_0; q_0 becomes smaller for increasing tensile stress.

In the following, we consider a graphene resonator with dimensions and parameters as given in Table I. We checked that the results do not change for larger values of the total length L. Using Eqs. (8) and (10), we obtain $\alpha/\alpha_0 \approx 0.64$ and $\tilde{\eta} \approx 7 \times 10^{-4}$. The latter implies bistable behavior of the resonator. In general, these values depend sensitively on the geometry of the graphene sheet and on the substrate. Our results provide a "best-case" estimate since the substrate is treated as a semi-infinite medium and the trench is modeled by the position-dependent coupling $K(x)$. Lifting these restrictions will lead to a stronger response of the substrate, and more dissipation.

A. Resonance frequency

As described in Sec. II A, the resonance frequency $\Omega_0(V_{dc})$ depends on the initial stress and the bias voltage. The dependence of Ω_0 on bias voltage, the so-called tuning curve, is a characteristic feature of NEMS devices. It is a result of the competition between softening (decreasing Ω_0) due to the electrostatic force [Eq. (15)], and stiffening (increasing Ω_0) due to the Duffing nonlinearity of the graphene sheet.

To obtain the tuning curve, we separate static and dynamic contributions to the displacement fields

$$w(x,t) = w_0(x) + \delta w(x,t)\,, \tag{16a}$$

$$u(x,t) = u_0(x) + \delta u(x,t) \tag{16b}$$

and insert these expressions into the equations of motion given by Eqs. (4). The static solutions w_0 and u_0 are calculated in Appendix B. Further, we expand the static force $f_{dc}(x)$ up to first order in δw:

$$f_{dc} \approx -\frac{\epsilon_0 V_{dc}^2}{2(d+w_0)^2} + \frac{\epsilon_0 V_{dc}^2}{(d+w_0)^3}\delta w. \tag{17}$$

The resonance frequency is then obtained by collecting terms, which are linear in the vibration amplitude δw. There are three such terms, which contribute to the resonance frequency:

$$\Omega_0^2(V_{dc}) = \Omega_0^2(0) + \Delta\Omega^2_{mech.} - \Delta\Omega^2_{el.} \tag{18a}$$

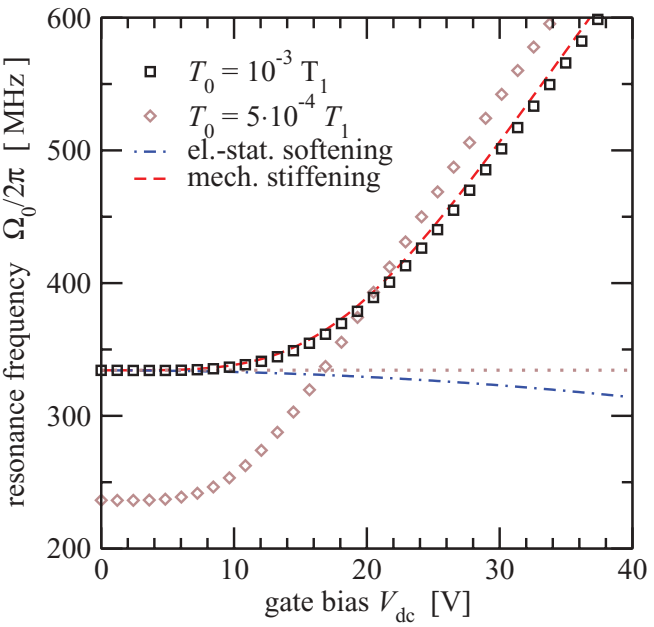

FIG. 2. (Color online) Resonance frequency Ω_0 vs bias voltage. Symbols denote results of numerical calculation. The dashed (red) and dashed-dotted (blue) lines show the contributions of mechanical stiffening and electrostatic softening for $T_0 = 10^{-3}T_1$, respectively. Parameters are given in Table I.

with

$$\Omega_0^2(0) = \frac{T_0}{\rho_G}\frac{\pi^2}{\ell^2}, \tag{18b}$$

$$\Delta\Omega^2_{mech.}(V_{dc}) = 2\frac{T_1\pi^4}{\rho_G\ell^4}q_0^2 = \frac{8}{3m}\alpha_0 q_0^2, \tag{18c}$$

$$\Delta\Omega^2_{el.}(V_{dc}) = \frac{\epsilon_0 V_{dc}^2}{d^3\rho_G}. \tag{18d}$$

The three contributions are due to initial strain, mechanical stiffening, and electrostatic softening, respectively. Since the static deflection q_0 depends on the bias voltage V_{dc}, the last two terms yield the voltage-dependent tuning behavior.

Figure 2 shows the tuning curve for the parameters given in in Table I. For voltages $V_{dc} > 10$ V, the resonance frequency (squared) is mainly determined by the mechanical stiffening, which scales with V_{dc}^4, while the softening term scales with V_{dc}^2 according to Eqs. (18).

Depending on the specific geometry and the initial stress, the resonance frequency of the resonator may be substantially tuned using the bias voltage. Since the linear and nonlinear damping coefficients given by Eqs. (8) depend on frequency, the magnitude of LD and NLD will, in principle, also be influenced by the tuning curve. In order to disentangle the influence of $\Omega_0(V_{dc})$ and the coupling to the in-plane phonons, we will only consider a constant resonance frequency $\Omega_0 = \Omega_0(0) = \sqrt{T_0/\rho_G}(\pi/\ell)$ in the following discussions (see Appendix C for the influence of the tuning on the quality factor).

B. Damping ratio

The relative importance of LD and NLD, which is quantified by $\tilde{\delta}$ defined in Eq. (9), is determined by the ratios

Im $\hat{\chi}(2\Omega)/[8\,\mathrm{Im}\,\hat{\chi}(\Omega)]$ and $|q_1^{\max}|/q_0$. The former weakly depends on the geometric details.

For small Ω, one can expand Im $\hat{\chi}(\Omega)$ in odd powers of Ω. As $\mathrm{Im}\hat{\chi}$ is proportional to the density of states of the substrate phonons, $D(\Omega) \propto \Omega$, we expect on symmetry grounds for a quasi-1D geometry that $\mathrm{Im}\hat{\chi}(\Omega) \propto \Omega^3$. Consistent with this expectation, we obtain numerically $\mathrm{Im}\hat{\chi}(2\Omega)/[8\,\mathrm{Im}\hat{\chi}(\Omega)] \approx 0.93$.

The maximum amplitude $q_1^{\max}$ can easily be found from Eq. (7) in the steady-state limit, which yields an implicit equation for the magnitude $|q_1|$ of the steady-state amplitude.[14] Sweeping the driving frequency, the maximum amplitude is attained when $d|q_1|/d\Omega = 0$, which results in the cubic equation

$$4\tilde{g} = |\tilde{q}_1^{\max}|\left(4\tilde{\gamma} + \tilde{\eta}|\tilde{q}_1^{\max}|^2\right). \tag{19}$$

Here, $\tilde{\gamma}$ and $\tilde{g}$ depend on the bias voltage V_{dc} via q_0 and f_{ac}, respectively. However, note that only $\tilde{g}$ depends on the ac voltage. Due to the different dependencies of q_0 and $|q_1^{\max}|$ on the bias voltage, one can achieve a crossover from NLD- to LD-dominated behavior by increasing the bias voltage. This is shown in Fig. 3(a). In the limit of small V_{dc}, $|\tilde{q}_1^{\max}| \approx (4\tilde{g}/\tilde{\eta})^{1/3} \propto V_{\mathrm{ac}}^{1/3} V_{\mathrm{dc}}^{1/3}$ and $\tilde{\delta} > 1$, i.e., NLD dominates. For large V_{dc}, $|\tilde{q}_1^{\max}| \approx \tilde{g}/\tilde{\gamma} \propto V_{\mathrm{ac}} V_{\mathrm{dc}}^{-3}$ and $\tilde{\delta}$ goes to zero with increasing V_{dc}. Since the static displacement is determined only by the geometry and the bias voltage, and the maximal amplitude additionally depends on the ac voltage, the crossover can also be realized by tuning V_{ac}, which is shown in Fig. 3(b). Equating the expressions for $|\tilde{q}_1^{\max}|$ in the two limits gives an estimate for the crossover for both voltages. Additionally, due to the dependencies of $q_0 \propto T_0^{-1}$ and $\Omega_0 \propto \sqrt{T_0}$ on the initial tension T_0, one finds that the damping ratio $\tilde{\delta}$ increases with increasing tension in both regimes ($\tilde{\delta} \propto T_0^3$ and $\tilde{\delta} \propto T_0$ in the LD and NLD regimes, respectively). Thus, the nonlinear damping is enhanced for larger T_0.

C. Quality factor

To quantify the energy loss, we consider the quality factor $Q = \Omega_0\langle E_\perp\rangle/\langle \dot{E}_\perp\rangle$, which measures the time-averaged dissipated energy $\langle \dot{E}_\perp\rangle$ normalized to the average energy $\langle E_\perp\rangle$ in the flexural modes. The nonlinearities render Q amplitude dependent. To get a worst-case estimate, we use the maximal amplitude. In the slow envelope approximation, we find

$$\frac{1}{Q} \approx \frac{\Omega_0\left(\gamma + \frac{1}{4}\eta|q_1^{\max}|^2\right)}{m\Omega_0^2 + \frac{1}{2}\frac{3}{8}\alpha|q_1^{\max}|^2}. \tag{20}$$

The nature of the damping influences Q. In the LD-dominated regime $\tilde{\delta} \ll 1$, Q is independent of the vibrational amplitude $Q_{\mathrm{LD}} \approx m\Omega_0/\gamma$. In contrast, for $\tilde{\delta} > 1$, one gets $Q_{\mathrm{NLD}} \approx 4m\Omega_0/(\eta|q_1^{\max}|^2)$ for $\tilde{\eta} > 1$. Thus, Q increases with decreasing driving strength. This agrees with the conclusions of Ref. 4.

Figure 4(a) shows the quality factor as a function of bias voltage for constant V_{ac}. As expected, Q decreases with increasing bias and excitation voltages and its behavior with regard to applied voltage changes qualitatively at the crossover between LD and NLD regimes. The asymptotic LD behavior limits the maximally attainable Q factor, which is indicated by the gray area. We also compare to the case where the LD is additionally caused by a mechanism that does not depend on the bias voltage leading to Q_0. In this case, the effective Q factor $Q_{\mathrm{eff}}^{-1} = Q^{-1} + Q_0^{-1}$ has a cutoff for small V_{dc} as shown in Fig. 4(b), which further limits the region of attainable Q factors. The qualitative difference between LD and NLD is still present and should be experimentally observable. Most importantly, by decreasing V_{ac}, the maximally attainable Q factor, which is determined by other damping mechanisms, can be approached.

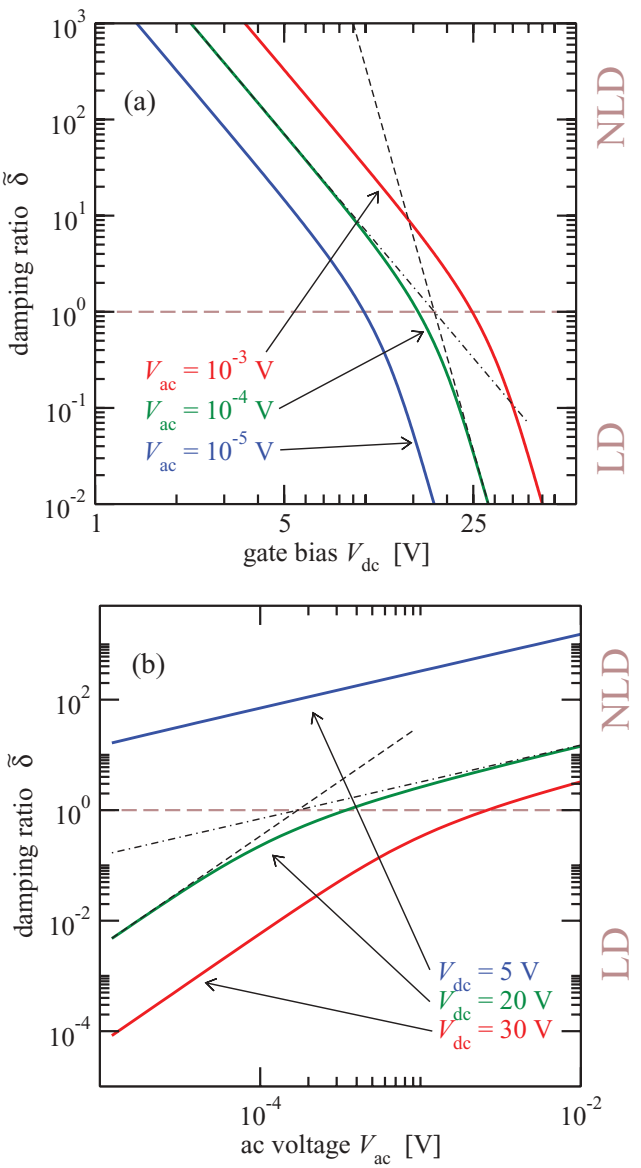

FIG. 3. (Color online) Ratio $\tilde{\delta}$ of nonlinear (NLD) and linear (LD) damping terms according to Eq. (9); (a) bias voltage and (b) ac voltage dependence. The thin dashed and dashed-dotted lines show the asymptotic behavior for strong LD and NLD. A crossover between the two regimes is achieved by changing the bias voltage. Parameters are given in Table I.

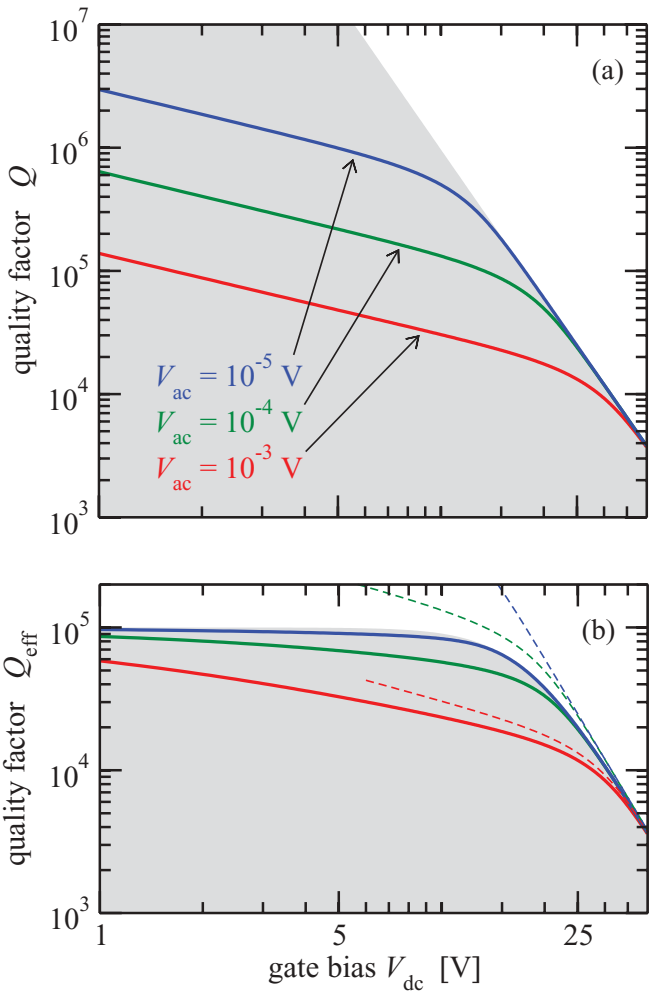

FIG. 4. (Color online) Quality factor Q vs bias voltage. (a) Q calculated from Eq. (20) and (b) with additional voltage-independent damping $Q_{\text{eff}}^{-1} = Q^{-1} + Q_0^{-1}$ with $Q_0 = 10^5$. The gray area indicates the region of attainable Q factors. The dashed lines correspond to the behavior in (a). Parameters are given in Table I.

IV. CONCLUSIONS

In conclusion, we have studied coupling between flexural vibrations and in-plane displacements as a physical mechanism for damping of flexural modes in graphene resonators. A characteristic consequence, which influences the behavior of the dependence of the quality factor on bias and excitation voltages, is the competition between static deflection and vibrational amplitude. We note that the same type of behavior would naturally occur for any dissipative process which couples linearly to the strain; for example, Ohmic dissipation induced by synthetic gauge fields.[19] The crossover should allow for an experimental verification of this class of damping mechanisms.

ACKNOWLEDGMENTS

We thank J. Atalaya for helpful discussions. The research leading to these results has received funding (D.M., A.I.) from the EU 7th framework program (FP7/2007-2013) RODIN (Grant Agreement No. 246026) and the Swedish Research Council (J.K.).

APPENDIX A: RESPONSE OF AN ELASTIC HALF-SPACE

The displacement response at the surface of an elastic half-space to a stress acting on the surface is given in terms of a response function by Eq. (3). If the stress is directed parallel to the x axis, the spatial Fourier transform of Eq. (3) reads as

$$u_S(\vec{k}, z = 0, \omega) = -R_{xx}(\vec{k}, \omega)\sigma_{xz}(\vec{k}, \omega), \tag{A1}$$

where $k = (k_x, k_y)$ is the surface wave vector in the surface. The response function $R_{xx}(\vec{k}, \omega)$ for finite frequencies is explicitly given by[30,31]

$$R_{xx}(\vec{k}, \omega) = -\frac{i}{\rho_S c_T^2}\left(\frac{p_T(\omega,k)}{S(\omega,k)}\frac{\omega^2}{c_T^2}\frac{k_x^2}{k^2} + \frac{1}{p_T(\omega,k)}\frac{k_y^2}{k^2}\right) \tag{A2a}$$

with

$$p_{L,T}(\omega,k) = \sqrt{\left(\frac{\omega}{c_{L,T}}\right)^2 + i\varepsilon - k^2}, \tag{A2b}$$

$$S(\omega,k) = \left[\left(\frac{\omega}{c_{L,T}}\right)^2 - 2k^2\right]^2 + 4k^2 p_L(\omega,k) p_T(\omega,k), \tag{A2c}$$

where c_L and c_T are the longitudinal and transversal speeds of sound, respectively, and the infinitesimal $\varepsilon > 0$ ensures causality. Notice that $p_{L,T}$ and $S(\omega,k)$ depend only on the modulus k of the wave vector $\vec{k}$. The response function in real space is then

$$\begin{aligned} R_{xx}(\vec{x}, \omega) &= \int d^2k R_{xx}(\vec{k}, \omega) e^{i\vec{k}\cdot\vec{x}} \\ &= -\frac{2\pi i}{\rho_S c_T^2}\left(\frac{\partial}{\partial x} I_x(x,y) + \frac{\partial}{\partial y} I_y(x,y)\right). \end{aligned} \tag{A3a}$$

Here, we defined

$$I_x(x,y) = \frac{x}{\sqrt{x^2+y^2}}\left(\frac{\omega}{c_T}\right)^2 \int dk\, \frac{p_T(\omega,k)}{S(\omega,k)} J_1(k\sqrt{x^2+y^2}), \tag{A3b}$$

$$I_y(x,y) = \frac{y}{\sqrt{x^2+y^2}} \int dk\, \frac{1}{p_T(\omega,k)} J_1(k\sqrt{x^2+y^2}), \tag{A3c}$$

where J_1 is a first-order Bessel function of the first kind. Note that

$$I_x(x,-y) = I_x(x,y), \quad I_y(x,-y) = -I_y(x,y). \tag{A4}$$

The expressions given in Eqs. (A3) are a very convenient starting point for the numerical evaluation of the response function used in Sec. II C.

The zero-frequency response can be directly calculated in real space.[24] One finds

$$R_{xx}(\vec{x}, \omega = 0) = \frac{1}{4\pi\rho_S c_T^2}\frac{2(c_T^2 - c_L^2)x^2 - c_L^2 y^2}{(c_L^2 - c_T^2)(x^2+y^2)^{3/2}}. \tag{A5}$$

APPENDIX B: STATIC DISPLACEMENT

In the static limit, the equations for the in-plane and out-of-plane displacements (4) within the suspended region become

$$T_1 u_{,xx} + \frac{T_1}{2}\partial_x\left(w_{,x}^2\right) = 0, \tag{B1a}$$

$$-\frac{T_1}{2}\partial_x\left[\left(2u_{,x} + w_{,x}^2\right)w_{,x}\right] = f_{\rm dc}, \tag{B1b}$$

with vanishing boundary conditions at $x = \pm\ell/2$ for the out-of-plane displacement. To find the proper boundary conditions for the in-plane displacement, we need to consider the coupling to the substrate in the nonsuspended region. Here, the equation for the in-plane displacement (4b) is given by

$$T_1 u_{,xx} - K(x)[u(x) - \overline{u}_S/b] = 0. \tag{B2}$$

Following the same line of reasoning as in the main text, the static substrate response can be written as

$$\overline{u}_{\rm S}(x) = -\int_{-L/2}^{L/2}\frac{dx'}{(2\pi)^2}\overline{R}_{xx}(x-x')\,\Theta(|x'|-\ell/2)h(x') \tag{B3}$$

with $h(x) = K_0(u - \overline{u}_S/b)$ and $\overline{R}_{xx}(x-x')$ being the static response function for an elastic half-space given by Eq. (A5) integrated over y. To treat the problem analytically, we convert Eqs. (B2) and (B3) into a local equation for the in-plane displacement. In the limit of very strong coupling to the substrate, the spatial variation of $h(x)$ is small, in which case

$$\begin{aligned}-\int_{-L/2}^{L/2}&\frac{dx'}{(2\pi)^2}\overline{R}_{xx}(x-x')\,\Theta(|x'|-\ell/2)h(x')\\ &\approx -h(x)\int_{-L/2}^{L/2}\frac{dx'}{(2\pi)^2}\overline{R}_{xx}(x-x')\Theta(|x'|-\ell/2).\end{aligned} \tag{B4}$$

This makes it possible to solve for $h(x)$ in terms of the in-plane displacement $u(x)$. One finds

$$h(x) = \frac{K_0}{1 - \overline{R}_0(x)K_0}u(x), \tag{B5}$$

where $\overline{R}_0(x) \equiv (2\pi)^{-2}\int_{-L/2}^{L/2}dx'\,\overline{R}_{xx}(x-x')\Theta(|x'|-\ell/2)$. This expression is valid outside the suspended region and is approximately given by $h(x) \approx -1/\overline{R}_0(x)$, which assumes $K_0\overline{R}_0(x) \gg 1$. Consequently, the equation for the in-plane displacement, Eq. (B2), is modified to become

$$T_1 u_{,xx} + \overline{R}_0(x)^{-1}u = 0 \tag{B6}$$

for $|x| > \ell/2$. Thus, the effect of the substrate is reduced to that of a spring with a spatially varying spring constant. The displacement u is expected to decay exponentially to zero in the clamped region with a decay length $\lambda \equiv \sqrt{\overline{R}_0(x)T_1}$. For the substrate parameters given in Table I, this amounts to $\lambda \approx 100$ nm. As a consequence, within a distance of 100 nm from the edge of the suspended region, the in-plane displacement $u(x)$ is essentially zero. To a good approximation, we therefore assume vanishing boundary conditions for in-plane displacement at $|x| = \ell/2$.

Setting $u(x) = (T_0/T_1)x + \Delta u(x)$, where the first terms account for initial strain in the graphene, the boundary conditions are $w(x = \pm\ell/2) = 0$ and $\Delta u(x = \pm\ell/2) = 0$.

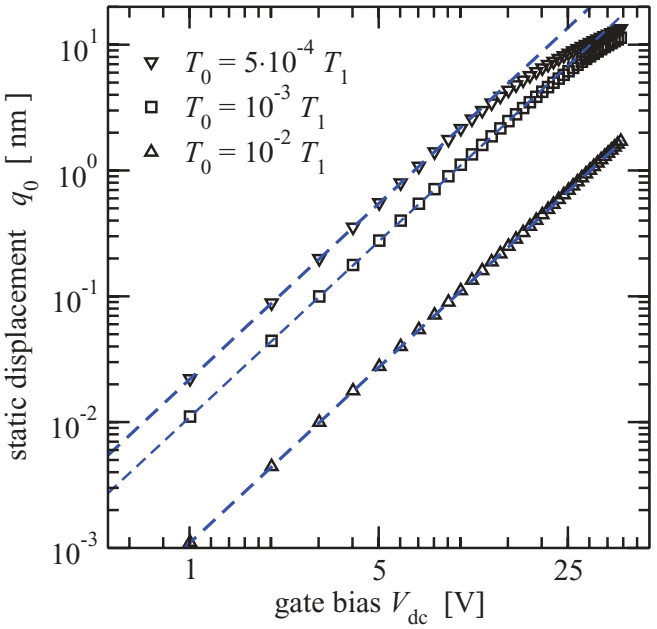

FIG. 5. (Color online) Static deflection q_0 vs bias voltage for three values of initial tension. The linear approximation [Eq. (B10)] is shown as dashed lines in the figure, while the squares and triangles correspond to the full numerical solution of the static problem.

Using the ansatz $w(x) = q_0\phi(x)$ with $\phi(x) = \sqrt{2}\cos\pi x/\ell$, the in-plane equation (B1a) reads as

$$\Delta u_{,xx} = -\frac{q_0^2}{2}\partial_x\left(\phi_{,x}^2\right). \tag{B7}$$

Consequently, the in-plane displacement will be given by

$$\Delta u(x) = -q_0^2\frac{\pi^2}{\ell^2}\int_0^x dx'\sin^2\pi x'/\ell + \frac{\pi^2}{2\ell^2}q_0^2 x\ . \tag{B8}$$

By inserting this expression into Eq. (B1b), we obtain

$$q_0\left(\frac{\pi^2}{\ell^2}T_0 + \frac{\pi^4}{2\ell^4}T_1 q_0^2\right) = \frac{2\sqrt{2}}{\pi}f_{\rm dc}. \tag{B9}$$

This is a purely algebraic equation for the static deflection. In the limit $q_0 \ll \frac{\ell}{\pi}\sqrt{\frac{T_0}{T_1}} \approx 10$ nm for $\ell = 1\ \mu$m and $T_0/T_1 = 10^{-3}$, the cubic term can be neglected and $q_0 \propto f_{\rm dc}$.

To compute q_0, we need to consider the electrostatic interaction with the back gate. The static force acting on the graphene is given by Eq. (15). Considering the limit $q_0 \ll d$, we obtain for the static displacement

$$q_0 = -\sqrt{2}\frac{\ell^2\epsilon_0 V_{\rm dc}^2}{\pi^3 T_0 d^2}, \tag{B10}$$

which is the expression given in Sec. III. In Fig. 5, the linear approximation (dashed line), given by Eq. (B10), is compared to the full numerical solution of Eq. (B1) (squares and triangles), which takes the substrate into account. The linear approximation remains valid in the displayed interval for the two larger values of initial strain T_0/T_1, while a more

significant deviation is apparent for the lowest value of the strain.

APPENDIX C: INFLUENCE OF TUNING AND INITIAL TENSION ON THE QUALITY FACTOR

In Sec. III A, we discussed the voltage dependence of the resonance frequency (tuning curve) and showed that the frequency can be substantially tuned by changing the bias voltage $V_{\rm dc}$. Since the linear and nonlinear damping constants given by Eqs. (8) depend on frequency, the quality factor will also depend on the tuning. In order to quantify the influence of the voltage dependence of the resonance frequency on Q, Fig. 6 shows the quality factor for constant $\Omega_0 = \Omega_0(0)$ (dashed lines) and $\Omega_0(V_{\rm dc})$ (full lines). One sees that deviations between these two cases appear only for larger voltages ($V_{\rm dc} > 20$ V). Moreover, the qualitative behavior and the crossover from NLD to LD behavior remains unchanged. This confirms our statement in Sec. III C that the behavior of Q is dominated by the damping coefficients γ and η rather than the voltage dependence of Ω_0.

Additionally, Fig. 6 shows the quality factor for a smaller value of the initial tension. In this case, the quality factor is decreased for all values of the static bias voltage. In the limit of large LD, this is due to the increased static deflection [see Eq. (B10)]. In the opposite limit, the quality factor is independent of the static deflection, and the decrease in quality factor is instead a result of the decreasing resonance frequency $\Omega_0(0) \propto \sqrt{T_0}$. Furthermore, as argued at the end of Sec. III B, the crossover between NLD and LD is shifted toward lower values of the bias voltage, signifying a decrease in the importance of NLD for lower tension.

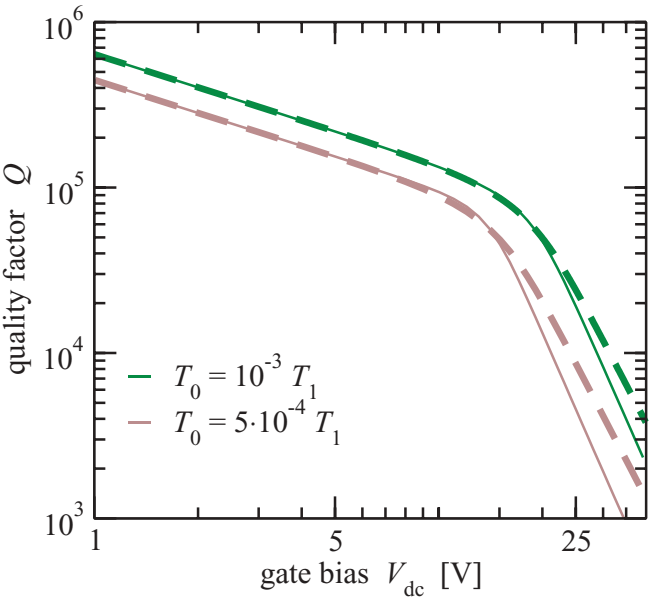

FIG. 6. (Color online) Quality factor Q vs bias voltage calculated from Eq. (20) for $V_{\rm ac} = 10^{-4}$ V. The full and dashed lines show the result for a voltage dependent $\Omega_0(V_{\rm dc})$ and constant $\Omega_0 = \Omega_0(0)$, respectively. Parameters are given in Table I.

*alexander.croy@chalmers.se

[1] J. S. Bunch, A. M. van der Zande, S. S. Verbridge, I. W. Frank, D. M. Tanenbaum, J. M. Parpia, H. G. Craighead, and P. L. McEuen, Science **315**, 490 (2007).

[2] A. Eriksson, S. Lee, A. A. Sourab, A. Isacsson, R. Kaunisto, J. M. Kinaret, and E. E. B. Campbell, Nano Lett. **8**, 1224 (2008).

[3] C. Chen, S. Rosenblatt, K. I. Bolotin, W. Kalb, P. Kim, I. Kymissis, H. L. Stormer, T. F. Heinz, and J. Hone, Nat. Nanotechnol. **4**, 861 (2009).

[4] A. Eichler, J. Moser, J. Chaste, M. Zdrojek, I. Wilson-Rae, and A. Bachtold, Nat. Nanotechnol. **6**, 339 (2011).

[5] R. Lifshitz and M. L. Roukes, Phys. Rev. B **61**, 5600 (2000).

[6] M. C. Cross and R. Lifshitz, Phys. Rev. B **64**, 085324 (2001).

[7] I. Wilson-Rae, Phys. Rev. B **77**, 245418 (2008).

[8] L. G. Remus, M. P. Blencowe, and Y. Tanaka, Phys. Rev. B **80**, 174103 (2009).

[9] C. Seoánez, F. Guinea, and A. H. Castro Neto, Phys. Rev. B **76**, 125427 (2007).

[10] A. D. O'Connell, M. Hofheinz, M. Ansmann, R. C. Bialczak, M. Lenander, E. Lucero, M. Neeley, D. Sank, H. Wang, M. Weides, J. Wenner, J. M. Martinis, and A. N. Cleland, Nature (London) **464**, 697 (2010).

[11] J. D. Teufel, T. Donner, D. Li, J. W. Harlow, M. S. Allman, K. Cicak, A. J. Sirois, J. D. Whittaker, K. W. Lehnert, and R. W. Simmonds, Nature (London) **475**, 359 (2011).

[12] A. Voje, J. M. Kinaret, and A. Isacsson, Phys. Rev. B **85**, 205415 (2012).

[13] M. Dykman and M. Krivoglaz, Sov. Sci. Rev., Sect. A **5**, 265 (1984).

[14] R. Lifshitz and M. Cross, *Nonlinear Dynamics of Nanomechanical and Micromechanical Resonators* (Wiley, New York, 2008), Chap. 1.

[15] S. Zaitsev, O. Shtempluck, E. Buks, and O. Gottlieb, Nonlinear Dynam. **67**, 859 (2012).

[16] R. Zwanzig, J. Stat. Phys. **9**, 215 (1973).

[17] K. Lindenberg and V. Seshadri, Phys. A (Amsterdam) **109**, 483 (1981).

[18] A. H. Castro Neto, F. Guinea, N. M. R. Peres, K. S. Novoselov, and A. K. Geim, Rev. Mod. Phys. **81**, 109 (2009).

[19] F. von Oppen, F. Guinea, and E. Mariani, Phys. Rev. B **80**, 075420 (2009).

[20] J. Sabio, C. Seoánez, S. Fratini, F. Guinea, A. H. Castro Neto, and F. Sols, Phys. Rev. B **77**, 195409 (2008).

[21] S. P. Koenig, N. G. Boddeti, M. L. Dunn, and J. S. Bunch, Nat. Nanotechnol. **6**, 543 (2011).

[22] S. Viola Kusminskiy, D. K. Campbell, A. H. Castro Neto, and F. Guinea, Phys. Rev. B **83**, 165405 (2011).

[23] *Statistical Mechanics of Membranes and Surfaces*, edited by D. Nelson, T. Piran, and S. Weinberg (World Scientific, Singapore, 1989).

[24] L. D. Landau and E. M. Lifshitz, *Theory of Elasticity*, 3rd ed., edited by A. M. Kosevich and L. P. Pitaevskiĭ (Butterworth-Heinemann, Oxford, 1986).

[25] B. I. Yakobson, C. J. Brabec, and J. Bernholc, Phys. Rev. Lett. **76**, 2511 (1996).

[26]A. Fasolino, J. H. Los, and M. I. Katsnelson, Nat. Mater. **6**, 858 (2007).
[27]J. Atalaya, A. Isacsson, and J. M. Kinaret, Nano Lett. **8**, 4196 (2008).
[28]N. Lindahl, D. Midtvedt, J. Svensson, O. A. Nerushev, N. Lindvall, A. Isacsson, and E. E. B. Campbell, Nano Lett. **12**, 3526 (2012).
[29]P. S. Swain and D. Andelman, Langmuir **15**, 8902 (1999).
[30]B. N. J. Persson, J. Chem. Phys. **115**, 3840 (2001).
[31]A. Maradudin and D. Mills, Ann. Phys. (NY) **100**, 262 (1976).
[32]A. W. Barnard, V. Sazonova, A. M. van der Zande, and P. L. McEuen, PNAS **109**, 19093 (2012).
[33]We found that $\overline{R}_{xx}(x-x',\omega)$ is well approximated by the integral $\int_{-b/2}^{b/2} dy R_{xx}(x-x',y,\omega)$.
[34]W. H. Press, B. P. Flannery, S. A. Teukolsky, and W. T. Vetterling, *Numerical Recipes in C: The Art of Scientific Computing* (Cambridge University Press, Cambridge, 1992), p. 994.
[35]C. Lee, X. Wei, J. W. Kysar, and J. Hone, Science **321**, 385 (2008).
[36]B. N. J. Persson and H. Ueba, Europhys. Lett. **91**, 56001 (2010).